Peer-reviewed version available at *Water* **2020**, *12*, 1245; doi:10.3390/w12051245

Article

Suppress Numerical Oscillations in Transient Mixed Flow Simulations with a Modified HLL Solver

Zhonghao Mao, Guanghua Guan, Zhonghua Yang

State Key Laboratory of Water Resources and Hydropower Engineering Science, Wuhan University, Wuhan, China.

* Correspondence: ggh@whu.edu.cn;

Abstract: Transition between free-surface and pressurized flows is an crucial phenomenon in many hydraulic systems, including water distribution systems, urban drainage systems, etc. During the transition, the force exerted on the structures changes drastically, thus it is meaningful to simulate this process. However, severe numerical oscillations are widely observed behind filling-bores, causing unphysical pressure variations and even computation failure. In this paper, some oscillation-suppressing approaches are reviewed and evaluated on a benchmark model. Then a new oscillation-suppressing approach is proposed to admit numerical viscosity when the water surface is at proximity of conduct roof which has first order accuracy. This approach adds numerical viscosity when water surface is at the proximity of conduct roof. It can sufficiently suppress numerical oscillations under an acoustic wave speed of 1000m/s and is simple to apply. In comparison with two experiments, the simulation results of this method show good agreement and little numerical oscillations. The results in this paper can help readers to choose an appropriate oscillation-suppressing method to improve the robustness and accuracy of flow regime transition simulations.

Keywords: flow regime transition, finite volume methods, numerical oscillations, numerical viscosity, Preissmann slot model

1. Introduction

Water, one of the most important living resources on earth, exists in our daily life under free-surface condition or pressurized condition. Under certain circumstances, transition between two flow regimes may occur; it is referred to as the flow regime transition phenomenon. The simulation results can support substantial information for the design and management of several common hydraulic systems, including but not limited to: rivers with crossing bridges or ice caps, drainage and irrigation tunnels, water distribution systems [1-7]. When the transition happens, the force that is exerted on the structures changes so violently that serious structural damage occurs [8-10]. Therefore, it is meaningful to simulate the transient pressure variations correctly when such transition happens.

The simulation of flow regime transition is a tricky problem because free-surface and pressurized flows are governed by different equations. To simplify this question, we can reduce the number of governing equations by adopting one set of governing equations for both flow conditions. Based on this idea, the Preissmann slot model (PSM) is proposed by Cunge [11] and it has been adopted by many researchers and commercial software packages for its simplicity and accuracy [12-18]. The gradient of piezometric head at the interface between two flow regimes are very steep which forms a discontinuity in flow, therefore the governing equations are normally discretized using the state-of-art finite volume method for it admits discontinuous solutions[19].

In the transient mixed flow simulations, numerical oscillations are widely observed behind the filling-bore front causing unphysical transient pressure peaks and computation failures [12]. These

numerical oscillations are very similar to the "post-shock oscillations" in gas dynamics which have been studied by many researchers [20-22]. It is pointed out that the numerical oscillations in transient mixed flow simulations have the same sources as the "post-shock oscillations" in gas dynamics [23]. In realistic situation, the flow states at two sides of a shock wave satisfy the Rankine-Hugoniot condition, while in the finite-volume methods, a shock wave spreads over several computational cells, and the flow states at two adjacent cells do not satisfy the Rankine-Hugoniot condition, this causes discrepancies in the wave information at each cell boundary. Previous research has shown that high order finite volume methods cause more numerical oscillations because of low dissipation away from shocks [21], first order upwind finite volume methods such as the Godunov type methods fail to prevent numerical oscillations [24], while centered finite volume methods like LxF or FORCE scheme may significantly smear data and compromise the representation of filling-bore front [23].

It needs to be noted that numerical oscillations do not only appear under the PSM, but also under other models, such as the two-component approach model and two equation model [25]. Many oscillation-suppressing methods have been proposed to solve this problem [12,23,24], however, there is no paper that evaluates the effects of these methods. In this paper, four oscillation-suppressing methods are tested on a benchmark model, their accuracy and robustness are rated, based on these approaches, a general idea to devise an oscillation-suppressing approach is revealed and then a new oscillation-suppressing method which can eliminate numerical oscillations under an acoustic wave speed of $1000ms^{-1}$ is proposed. This paper is arranged as follows: In section 2, we introduce a benchmark model which was adopted by Malekpour and Karney [24]. In section 3, some oscillation-suppressing methods are reviewed, their theories are illustrated and their effects are evaluated. In section 5, a new and simple modified HLL solver to suppress numerical oscillations is proposed. In section 6, the accuracy and robustness of this solver are validated against two experiments. Conclusions are drawn in the last section.

2. Governing equations and discretization method

In the PSM, pressurized flow is transformed into free-surface flow by positing a narrow slot at the top of cross-sections so that the piezometric head in two flow regimes can be represented by water depth, as shown in **Fig 1**. The slot width needs to be very small so that the gravity wave speed inside it is identical with acoustic wave speed.

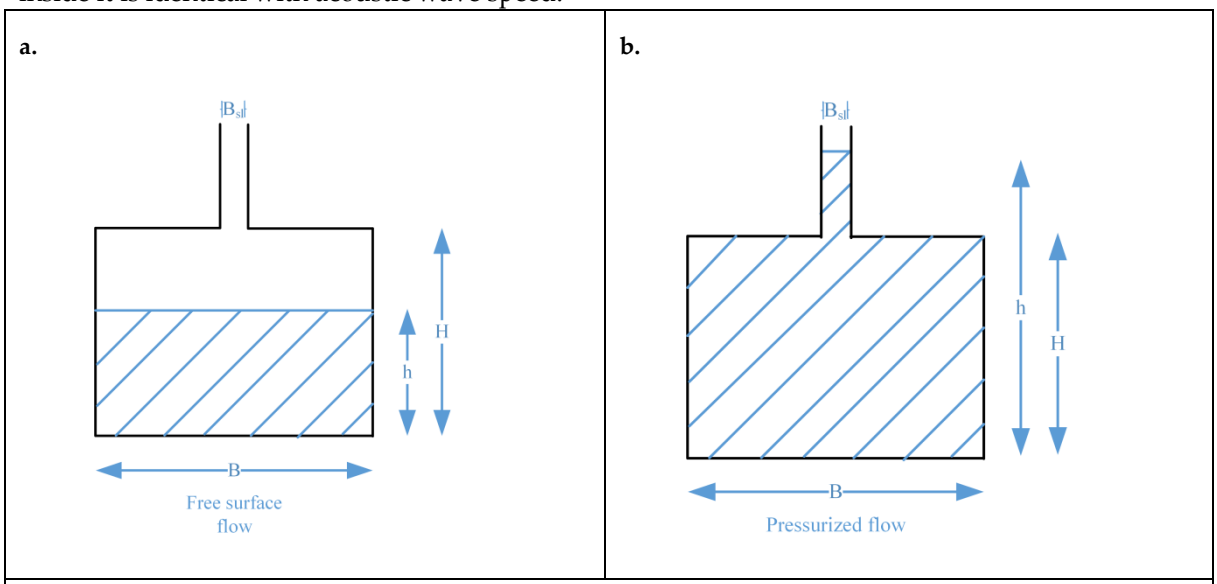

Fig 1. A rectangular pipe which is modified by the PSM, a. under free surface flow condition, b. under pressurized flow condition

Under the framework of PSM, the governing equations of one dimensional free-surface and pressurized flows in prismatic conducts can be written in the conservation laws form [26]:

Preprints (www.preprints.org) | NOT PEER-REVIEWED | Posted: 24 February 2020 doi:10.20944/preprints202002.0344.v1

Peer-reviewed version available at Water 2020, 12, 1245; doi:10.3390/w12051245

$$\frac{\partial \mathbf{U}}{\partial t}+\frac{\partial \mathrm{F}(\mathbf{U})}{\partial x}=\mathrm{S}(\mathbf{U}),$$

$$\mathbf{U}=\begin{pmatrix}A\\Q\end{pmatrix},\mathrm{F}(\mathbf{U})=\begin{pmatrix}Q\\\frac{Q^2}{A}+gI(h)\end{pmatrix},\mathrm{S}(\mathbf{U})=\begin{pmatrix}0\\gA(S_b-S_f)\end{pmatrix}, \tag{1}$$

$$I(h)=\int_0^h(h-\xi)l(x,\xi)d\xi$$

Where Q is the volume flow rate, A is the wetted cross-sectional area, g is the acceleration of gravity, h is the water depth, l is the cross-sectional width with $l(x, h) = b(x)$ the water surface width, S_0 is the bed slope, S_f is the friction slope which reflects the friction of bed and wall acting on flow, it can be computed using the Manning relation:

$$S_f=\frac{n^2u|u|}{R^{4/3}} \tag{2}$$

Where u is the flow velocity, n is the Manning coefficient, R is the hydraulic radius. For a rectangular cross-section with the slot on its top, b, A and I can be expressed as functions of h:

$$b(h)=\begin{cases}B, & h\le H\\B_{sl}, & h>H\end{cases} \tag{3}$$

$$A(h)=\begin{cases}Bh, & h\le H\\BH+B_{sl}(h-H), & h>H\end{cases} \tag{4}$$

$$I(h)=\begin{cases}0.5*Bh^2, & h\le H\\BH*(h-0.5H)+0.5*B_{sl}(h-H)^2, & h>H\end{cases} \tag{5}$$

Where H and B are the cross-sectional height and width, B_{sl} is the width of slot. In order to make the gravity wave speed in accordance with the acoustic wave speed a, the slot width $B_{sl} = g\,a^{-2}A_f$, where A_f is the full cross-sectional area of conduct and a is the acoustic wave speed [27]. Using the Godunov-type finite volume methods with first order accuracy, the governing equations are discretized as:

$$\mathbf{U}_i^{n+1}=\mathbf{U}_i^n-\frac{\Delta t_i}{\Delta x_i}(\mathbf{F}_{i+1/2}-\mathbf{F}_{i-1/2}) \tag{6}$$

$$\mathbf{U}_i^n=\frac{1}{\Delta x_i}\int_{x_{i-1/2}}^{x_{i+1/2}}\mathbf{U}(x,t^n)dx,\ \mathbf{U}_i^{n+1}=\frac{1}{\Delta x_i}\int_{x_{i-1/2}}^{x_{i+1/2}}\mathbf{U}(x,t^{n+1})dx \tag{7}$$

$$\mathbf{F}_{i-1/2}=\frac{1}{\Delta t_i}\int_{t^n}^{t^{n+1}}\mathrm{F}(\mathbf{U}(x_{i-1/2},t))dt,\ \mathbf{F}_{i+1/2}=\frac{1}{\Delta t_i}\int_{t^n}^{t^{n+1}}\mathrm{F}(\mathbf{U}(x_{i+1/2},t))dt \tag{8}$$

Preprints (www.preprints.org) | NOT PEER-REVIEWED | Posted: 24 February 2020 doi:10.20944/preprints202002.0344.v1

Peer-reviewed version available at Water 2020, 12, 1245; doi:10.3390/w12051245

3. Review to current oscillation-suppressing approaches

The benchmark model was proposed by Malekpour and Karney [24], it consists of a conduct with unit square cross-sections which is connected to a reservoir at the upstream end while the flow states at downstream end are unchanged. Under initial condition, 0.6m-deep stagnant water is in the conduct while the water level inside the reservoir is constant 4m as shown in **Fig 2**:

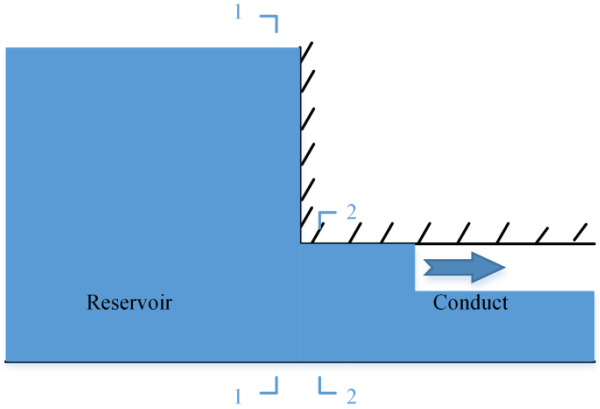

Fig 2. Front view of the benchmark model.

Where 1-1 and 2-2 are two cross-sections immediately upstream and downstream of the interface between reservoir and conduct. Under initial condition, flow states $\mathbf{U}_L$ and $\mathbf{U}_R$ in the conduct and reservoir are discontinuous which forms a dam break problem with geometric discontinuity at the interface:

$$\begin{bmatrix} h_L \\ u_L \end{bmatrix} = \begin{bmatrix} 4m \\ 0m/s \end{bmatrix}, \begin{bmatrix} h_R \\ u_R \end{bmatrix} = \begin{bmatrix} 0.6m \\ 0m/s \end{bmatrix} \tag{9}$$

The flow sates behind the filling-bore can be obtained by solving the following equations iteratively [24]:

$$h_1 = h_2 + \frac{u_2^2}{2g} \tag{10}$$

$$u_2 = u_R + \sqrt{\frac{\left[gI(A_R) - gI(A_2)\right](A_R - A_2)}{A_R A_2}} \tag{11}$$

Then a ghost cell is set at the upstream boundary adopting u_2 and A_2. Since $\mathbf{U}_2$ are connected to $\mathbf{U}_R$ through a right shock, flow states inside the conduct will be replaced by $\mathbf{U}_2$ ultimately, which gives the analytical solution in this model. We study a mixed flow inside a this conduct, the acoustic wave speed is assumed to be constant $1000ms^{-1}$ and the according slot width is $9.8\times10^{-6}m$. The size of each computational cell is 1m, the time step is 0.008s and the Courant number is 0.8.

Numerical Filtering Methods

Vasconcelos et al [23] proposed to suppress the numerical oscillations by smearing the flow states among three conjunct cells at each time step. The exact Riemann solver is adopted to solve the Riemann problem at each cell boundary. The flow states $\mathbf{U}_{i+1/2}$ at $x_{i+1/2}$ satisfy the following equations:

Preprints (www.preprints.org) | NOT PEER-REVIEWED | Posted: 24 February 2020 doi:10.20944/preprints202002.0344.v1

Peer-reviewed version available at Water 2020, 12, 1245; doi:10.3390/w12051245

$$u_{i+1/2}\left(A_{i+1/2}\right)=\begin{cases} u_i-\sqrt{\dfrac{\left[gI\left(A_i\right)-gI\left(A_{i+1/2}\right)\right]\left(A_i-A_{i+1/2}\right)}{A_iA_{i+1/2}}}, & A_{i+1/2}>A_i \\ u_i+\int_0^{A_L}\sqrt{\dfrac{g}{\alpha b}}d\alpha-\int_0^{A_{i+1/2}}\sqrt{\dfrac{g}{\alpha b}}d\alpha, & A_{i+1/2}<A_i \end{cases} \tag{12}$$

$$u_{i+1/2}\left(A_{i+1/2}\right)=\begin{cases} u_{i+1}+\sqrt{\dfrac{\left[gI\left(A_{i+1}\right)-gI\left(A_{i+1/2}\right)\right]\left(A_{i+1}-A_{i+1/2}\right)}{A_{i+1}A_{i+1/2}}}, & A_{i+1/2}>A_{i+1} \\ u_{i+1}-\int_0^{A_{i+1}}\sqrt{\dfrac{g}{\alpha b}}d\alpha+\int_0^{A_{i+1/2}}\sqrt{\dfrac{g}{\alpha b}}d\alpha, & A_{i+1/2}<A_{i+1} \end{cases} \tag{13}$$

The solution to $\mathbf{U}_{i+1/2}$ can be obtained by solving equations (12) and (13) iteratively, although the exact solver can compute the wave structure in each Riemann problem correctly, there are serious numerical oscillations in the simulation results. A filtering process is carried out after flow sates are updated in all computational cells,:

$$\mathbf{U}_i^{n+1,f}=\left(1-2\varepsilon\right)\mathbf{U}_i^{n+1}+\varepsilon\left(\mathbf{U}_{i-1}^{n+1}+\mathbf{U}_{i+1}^{n+1}\right) \tag{14}$$

The authors suggest ε to be between 0.025 and 0.050. This method is easy to implement, however, as pointed by the author, it will increase the spreading length of filling-bore front and remove any physical oscillations that appear in the solution, thus it is suitable only for limited applications. On the benchmark model, this method produces very unstable results using ε = 0.04, the simulation results are depicted in Fig 3.

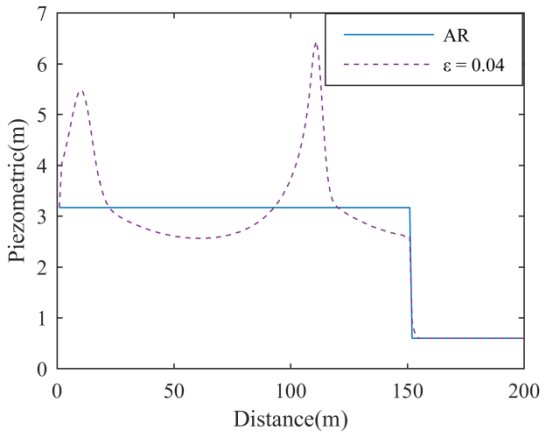

Fig 3. Simulation results of numerical filtering methods and analytical solution.

Hybrid Flux Approach

Another two oscillation-suppressing approaches are sorted as hybrid fluxes because they use two numerical fluxes alternatively. The first one is based on the Roe solver [28] and the LxF scheme [23]. The Roe solver is written as:

$$\mathbf{F}_{i+1/2}^{\text{Roe}} = \frac{1}{2}\left[\mathrm{F}\left(\mathbf{U}_{i+1}^{n}\right)+\mathrm{F}\left(\mathbf{U}_{i}^{n}\right)\right]-\frac{1}{2}\sum_{j=1}^{2}\left|\lambda_{i+1/2}^{j}\right|\alpha_{i+1/2}^{j}\mathbf{R}_{i+1/2}^{j} \tag{15}$$

Where $\lambda_{i+1/2}^{j}$ are eigenvalues of the linearized Jacobian matrix, $\mathbf{R}_{i+1/2}^{j}$ are the corresponding right eigenvectors, $\alpha_{i+1/2}^{j}$ are wave strengths across cell boundary. They are expressed as:

$$\lambda_{i+1/2}^{1} = \frac{\overset{\circ}{Q}_{i+1/2}}{\overset{\circ}{A}_{i+1/2}} - \overset{\%}{c}_{i+1/2}, \lambda_{i+1/2}^{2} = \frac{\overset{\circ}{Q}_{i+1/2}}{\overset{\circ}{A}_{i+1/2}} + \overset{\%}{c}_{i+1/2} \tag{16}$$

$$\mathbf{R}_{i+1/2}^{1} = \left[1, \lambda_{i+1/2}^{1}\right]^{T}, \mathbf{R}_{i+1/2}^{2} = \left[1, \lambda_{i+1/2}^{2}\right]^{T} \tag{17}$$

$$\alpha_{i+1/2}^{1} = \frac{\lambda_{i+1/2}^{2}\left(A_{i+1}-A_{i}\right)-\left(Q_{i+1}-Q_{i}\right)}{\lambda_{i+1/2}^{2}-\lambda_{i+1/2}^{1}}, \alpha_{i+1/2}^{2} = \frac{\left(Q_{i+1}-Q_{i}\right)-\lambda_{i+1/2}^{1}\left(A_{i+1}-A_{i}\right)}{\lambda_{i+1/2}^{2}-\lambda_{i+1/2}^{1}} \tag{18}$$

Where $\overset{\circ}{Q}_{i+1/2}$, $\overset{\circ}{A}_{i+1/2}$ and $\overset{\%}{c}_{i+1/2}$ are Roe averages:

$$\overset{\circ}{A}_{i+1/2} = \left(A_{i}A_{i+1}\right)^{1/2} \tag{19}$$

$$\overset{\circ}{Q}_{i+1/2} = \frac{\left(A_{i}\right)^{1/2}Q_{i+1}+\left(A_{i+1}\right)^{1/2}Q_{i}}{\left(A_{i}\right)^{1/2}+\left(A_{i+1}\right)^{1/2}} \tag{20}$$

$$\overset{\%}{c}_{i+1/2} = \begin{cases} \left[g\dfrac{I\left(A_{i+1}\right)-I\left(A_{i}\right)}{A_{i+1}-A_{i}}\right]^{1/2}, & A_{i+1}\neq A_{i} \\ \left[g\dfrac{A_{i}+A_{i+1}}{b_{i}+b_{i+1}}\right]^{1/2}, & A_{i+1}=A_{i} \end{cases} \tag{21}$$

The Roe solver is known vulnerable to numerical oscillations [21,29], while the LxF scheme is robust against numerical oscillations but it is too diffusive at free-surface regimes. To take the advantages of two schemes, Vasconcelos et al [23] proposed a hybrid flux, it imitates the LxF scheme at the cell boundary between two flow regimes, at other cell boundaries, it acts like the Roe solver:

$$\left|\lambda_{i+1/2}^{1,2}\right| = \min\left[\frac{\Delta x}{\Delta t}, \left|\frac{\overset{\circ}{Q}_{i+1/2}}{\overset{\circ}{A}_{i+1/2}} \mathrm{m} \overset{\%}{c}_{i+1/2}\right| + L\left(\Delta c_{i+1/2}\right)^{L}\frac{\Delta x}{\Delta t}\right] \tag{22}$$

$$\Delta c_{i+1/2} = \frac{\left|\overset{\%}{c}_{i+1}-\overset{\%}{c}_{i}\right|}{\max\left(\left|\overset{\%}{c}_{i+1}-\overset{\%}{c}_{i}\right|\right)_{i=1\ldots N-1}} \tag{23}$$

$\Delta c_{i+1/2} = 1$ at the cell boundary between free-surface and pressurized flow regimes, the parameter L ranges from o to 1, when it changes from 1 to 0, equation (22) switches from the Roe solver to the LxF scheme the cell boundary between free-surface and pressurized regimes. At other cell boundaries, it acts like the Roe solver. In this way, numerical viscosity is added at the cell

boundary where flow condition transition happens, while its amount increases with L. The simulation results of the hybrid flux with L = 0.6 are drawn in Fig 4. This flux overestimates the spreading length of filling-bore like other centered finite volume methods, which indicates that excessive numerical viscosity is added at the cell boundary between two flow regimes. Meanwhile, it fails to suppress the numerical oscillations on the benchmark model under an acoustic wave speed of 1000m/s.

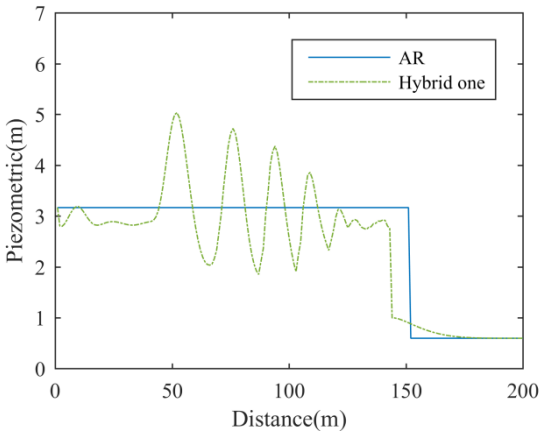

Fig 4. Simulation results of hybrid flux approach and analytical result (AR).

Hyunuk et al [12] also provided a hybrid flux, it uses the FORCE scheme at the cell boundary between free-surface and pressurized flows and HLL solver elsewhere so that numerical viscosity is only added in there:

$$\mathbf{F}_{i+1/2}^{\text{hybrid}} = \begin{cases} \mathbf{F}_{i+1/2}^{\text{FORCE}}, & (h_L - H_L)(h_R - H_R) < 0 \\ \mathbf{F}_{i+1/2}^{\text{HLL}}, & \text{otherwise} \end{cases} \tag{24}$$

The HLL solver assumes the two waves in the Riemann problem are shock waves and then their wave speeds S_{wL} and S_{wR} can be obtained making use of the Rankine-Hugoniot condition:

$$S_{wL} = \frac{\mathrm{F}(\mathbf{U}_i) - \mathrm{F}(\mathbf{U}_{i+1/2})}{\mathbf{U}_i - \mathbf{U}_{i+1/2}}, S_{wR} = \frac{\mathrm{F}(\mathbf{U}_{i+1}) - \mathrm{F}(\mathbf{U}_{i+1/2})}{\mathbf{U}_{i+1} - \mathbf{U}_{i+1/2}} \tag{25}$$

In addition, an approximate Riemann solver is needed to compute $\mathbf{U}_{i+1/2}$ [30]. We adopt the one proposed by Leno et al [31] which is meant to admit the minimum amount of numerical viscosity:

$$A_{i+1/2} = \frac{A_i + A_{i+1}}{2}\left(1 + \frac{u_i - u_{i+1}}{\sqrt{g\frac{A_i}{b_i}} + \sqrt{g\frac{A_{i+1}}{b_{i+1}}}}\right) \tag{26}$$

The solution is substituted into equation (25):

$$S_{wL} = u_i - \Omega_i, S_{wR} = u_{i+1} + \Omega_{i+1} \tag{27}$$

Preprints (www.preprints.org) | NOT PEER-REVIEWED | Posted: 24 February 2020 doi:10.20944/preprints202002.0344.v1

Peer-reviewed version available at Water 2020, 12, 1245; doi:10.3390/w12051245

$$\Omega_{K(K=i,i+1)}=\begin{cases}\sqrt{g\dfrac{\left[I\left(A_{i+1/2}\right)-I\left(A_K\right)\right]A_{i+1/2}}{A_K\left(A_{i+1/2}-A_K\right)}}, & A_{i+1/2}>A_K\\ \sqrt{g\dfrac{A_K}{b_K}}, & A_{i+1/2}\le A_K\end{cases}$$

The choice of HLL fluxes are based on the direction of shock wave:

$$\mathbf{F}_{i+1/2}^{\mathrm{HLL}}=\begin{cases}\mathrm{F}\left(\mathbf{U}_i\right), & S_{wL}>0\\ \mathrm{F}\left(\mathbf{U}_{i+1/2}\right), & S_{wL}\le 0\ \&\ S_{wR}\ge 0\\ \mathrm{F}\left(\mathbf{U}_{i+1}\right), & S_{wR}<0\end{cases} \tag{28}$$

F ($\mathbf{U}_{i+1/2}$) is derived after cancelling $\mathbf{U}_{i+1/2}$ in Equ (25):

$$\mathrm{F}\left(\mathbf{U}_{i+1/2}\right)=\frac{S_{wR}\,\mathrm{F}\left(\mathbf{U}_i\right)-S_{wL}\,\mathrm{F}\left(\mathbf{U}_{i+1}\right)+S_{wR}S_{wL}\left(\mathbf{U}_{i+1}-\mathbf{U}_i\right)}{S_{wR}-S_{wL}} \tag{29}$$

The FORCE flux is given by the algebraic average of LxF scheme and Lax-Wendorff scheme [32]. It is a diffusive scheme thus it is efficient in suppressing numerical oscillations, meanwhile, it is less diffusive than the LxF flux which can reduce the over-smearing at strong gradients [33].

$$\mathbf{F}_{i+1/2}^{\mathrm{LW}}=\mathrm{F}\left(\mathbf{U}_{i+1/2}^{\mathrm{LW}}\right),\mathbf{U}_{i+1/2}^{\mathrm{LW}}=\frac{1}{2}\left(\mathbf{U}_i^n+\mathbf{U}_{i+1}^n\right)-\frac{\Delta x}{2\Delta t}\left[\mathrm{F}\left(\mathbf{U}_{i+1}^n\right)-\mathrm{F}\left(\mathbf{U}_i^n\right)\right],$$

$$\mathbf{F}_{i+1/2}^{\mathrm{LxF}}=\frac{1}{2}\left[\mathrm{F}\left(\mathbf{U}_{i+1}^n\right)+\mathrm{F}\left(\mathbf{U}_i^n\right)\right]-\frac{\Delta x}{2\Delta t}\left(\mathbf{U}_{i+1}-\mathbf{U}_i\right), \tag{30}$$

$$\mathbf{F}_{i+1/2}^{\mathrm{FORCE}}=\frac{1}{2}\left(\mathbf{F}_{i+1/2}^{\mathrm{LW}}+\mathbf{F}_{i+1/2}^{\mathrm{LxF}}\right)$$

The simulation results are depicted in **Fig 5**.

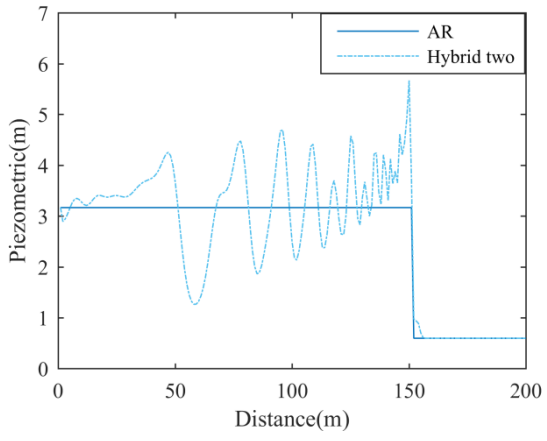

Fig 5. Simulation results of hybrid flux approach and analytical result (AR).

The two hybrid flux approaches are quite similar; they choose a diffusive flux at the cell boundary between two flow regimes, while at other cell boundaries, an upwind flux is adopted to introduce minimum numerical viscosity. However, they both fail to suppress the numerical oscillations on the benchmark model, under an acoustic wave speed of 1000m/s. **Fig 4** shows that although excessive numerical viscosity at the cell boundary between two flow regimes, the numerical oscillations still persist.

Preprints (www.preprints.org) | NOT PEER-REVIEWED | Posted: 24 February 2020 doi:10.20944/preprints202002.0344.v1

Peer-reviewed version available at Water 2020, 12, 1245; doi:10.3390/w12051245

Modified HLL Solver

Numerical viscosity can efficiently suppress the numerical oscillations, however, one needs to add appropriate amount of numerical viscosity otherwise the spreading length of bore front will be over-estimated. Malekpour and Karney [24] pointed out that the amount of numerical viscosity in upwind methods increase with the estimates of wave speed in equation (29), when S_{wL} and S_{wR} equal $\Delta x/\Delta t$, the very diffusive LxF scheme is reproduced. The authors proposed an approximate Riemann solver, in which $h_{i+1/2}$ is decided by the largest piezometric head within a couple of surrounding cells:

$$h_{i+1/2} = K_a * \max\left(h_{i-NS}, h_{i-NS+1}, \mathrm{L}\ , h_{i-1}, h_i, h_{i+1}, \mathrm{L}\ , h_{i+NS-1}, h_{i+NS}\right) \tag{31}$$

The two parameters $K_a > 1$ and $NS \geq 3$. When the piezometric head at the surrounding cells is near the conduct roof, equation (31) produces a result of $h_{i+1/2}$ higher than the conduct roof. Meanwhile, the authors pointed out that a $h_{i+1/2}$ larger than cross-sectional height makes equation (27) provide a wave speed that is not very different from the gravity wave speed except at the vicinity of conduct roof. In this way, numerical viscosity is added at the cell when the piezometric head at its vicinity is near the conduct roof. The simulation results of K_a =1.6 and NS = 5 are drawn in **Fig 6**.

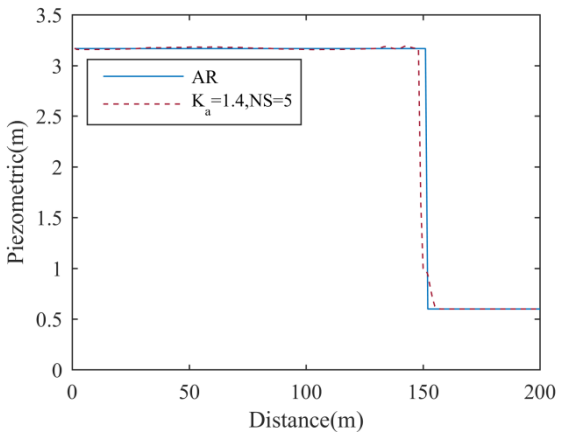

Fig 6. Simulation results of modified HLL solver and the analytical result (AR).

Unlike the hybrid flux approaches, the modified solver adds numerical viscosity at multiple cells at the vicinity of the filling-bore front. Although the amount of numerical viscosity is far smaller than the hybrid flux approaches, it can suppress numerical oscillations on the benchmark model. Meanwhile, because this solver admits numerical viscosity at theses free-surface cells, it slightly increases the spreading length of filling-bore front. Compared to its oscillations-suppressing effect, this flaw is general acceptable. However, the two parameters in this solver demand a tuning process which hinders its application under realistic situations.

4. A new modified HLL solver

In this section, we present a new modified HLL solver to suppress the numerical oscillations, it is as efficient as the former one but is more convenient to use. In this solver, the solution to $h_{i+1/2}$ is given under two situations:

Preprints (www.preprints.org) | NOT PEER-REVIEWED | Posted: 24 February 2020 doi:10.20944/preprints202002.0344.v1

Peer-reviewed version available at Water 2020, 12, 1245; doi:10.3390/w12051245

$$A_{i+1/2} = \begin{cases} P_a * H, & h_i > P_b * H | h_{i+1} > P_b * H \\ \frac{A_i + A_{i+1}}{2}\left(1 + \frac{u_i - u_{i+1}}{\sqrt{g\frac{A_i}{b_i}} + \sqrt{g\frac{A_{i+1}}{b_{i+1}}}}\right), & else \end{cases} \quad (32)$$

When the water depths at cell i and i+1 are lower than a certain ratio (P_b) of cross-sectional depth H, equation (26) is adopted to admit minimum amount of numerical viscosity. As the water depths in two cells reach the proximity of conduct roof, we assume that flow condition transition is about to happen and the solution of $h_{i+1/2}$ is constantly $P_a * H$ which is larger than the highest piezometric head so that equation (27) can produce a larger wave speed and numerical viscosity is added. The two parameters P_a and P_b need to be defined by the users in advance, P_b must be smaller than one, a suggested value is between 0.7 and 0.9, while $P_a * H$ needs to be larger than the highest piezometric head during the transient mixed flow phenomenon as stated before.

The amount of numerical viscosity increases with the value of P_a but it is not sensitive to it. As a matter of fact, to make the modified solver as diffusive as the LxF scheme, P_a needs to be as large as 25000 to make equation (27) produce a wave speed that equals $\Delta x/\Delta t$ on the benchmark model. Under realistic applications, one can always adopt a P_a that is sufficiently larger than the possible highest piezometric head without compromising the representation of filling-bore significantly. The simulation results of the modified HLL solver under different values of P_a and P_b are drawn in Fig 7:

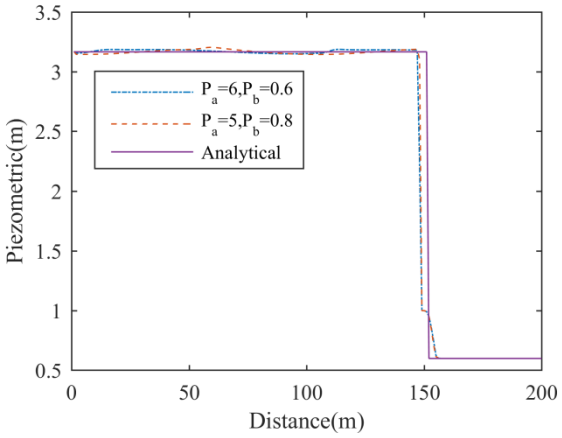

Fig 7. Simulation results of the new modified HLL solver under different values of P_a and P_b.

5. Numerical tests

5.1. Test case 1

This test is meant to evaluate the accuracy of two modified HLL solvers under the presence of two filling-bores. It is conducted a 100m-long conduct with unit square cross-sections under an acoustic wave speed of 1000ms^{-1}; two reservoirs are connected to the conduct at the upstream end and downstream end. At initial condition, water in the conduct is stationary with a depth of 0.6m, while the water depths at the upstream reservoir and downstream reservoir are 4m and 3m, respectively. At t = 0s, the two gates separating the reservoirs and the conduct are suddenly opened, forming two filling-bores that propagates in the opposite direction. The flow states and propagation speed of filling-bore at upstream boundary can be derived following equations (10) and (11), while those at the downstream boundary can be obtained by:

Preprints (www.preprints.org) | NOT PEER-REVIEWED | Posted: 24 February 2020 doi:10.20944/preprints202002.0344.v1

Peer-reviewed version available at Water 2020, 12, 1245; doi:10.3390/w12051245

$$\begin{bmatrix} h_L \\ u_L \end{bmatrix} = \begin{bmatrix} 0.6m \\ 0m/s \end{bmatrix}, \begin{bmatrix} h_R \\ u_R \end{bmatrix} = \begin{bmatrix} 3m \\ 0m/s \end{bmatrix} \tag{33}$$

$$h_1 = h_2 + \frac{u_2^2}{2g} \tag{34}$$

$$u_L - \sqrt{\frac{\left[gI(A_L) - gI(A_2)\right](A_L - A_2)}{A_L A_2}} \tag{35}$$

At the downstream end, 1-1 is the first cross-section in the reservoir and 2-2 is the last cross-section in the conduct. Two tests are conducted, the first test adopts the modified HLL solver proposed in this paper. The highest piezometric head in this case is 3.167m, while initially the water depth is 0.6 times of the cross-sectional height, accordingly, we choose P_a = 5 and P_b = 0.8. The second test adopts the modified HLL solver proposed by Malekpour et al, the values of K_a and NS are 1.4 and 5 as suggested by the authors.

In two tests, the simulation area is divided into 100 computational cells; the time step is set for a Courant number of 0.8. The simulation results in two tests at t = 3s are drawn in **Fig 8**. In this paper, an error indicator based on L_2-norm [34] is used to evaluate the accuracy of simulation results in comparison with the analytical result, in the following equation, h_i stands for the piezometric head at ith cell in simulation result, while h_{ref} stands for the analytical result.

$$L_2 = \left(\frac{1}{N} \sum_{i=1}^{N} \left(h_i - h_{\text{ref}} \right)^2 \right)^{0.5} \tag{1}$$

The L_2 of test one and two are 0.5405 and 0.5646, respectively. In test 1, the spreading length of the right filling-bore front is slightly longer than that in test 2, which denotes that the modified solver proposed in this paper is more diffusive at the right filling-bore. At the same time, the solver proposed in this paper has eliminated some minor numerical oscillations while the other one doesn't. After all, both solvers are very robust and stable.

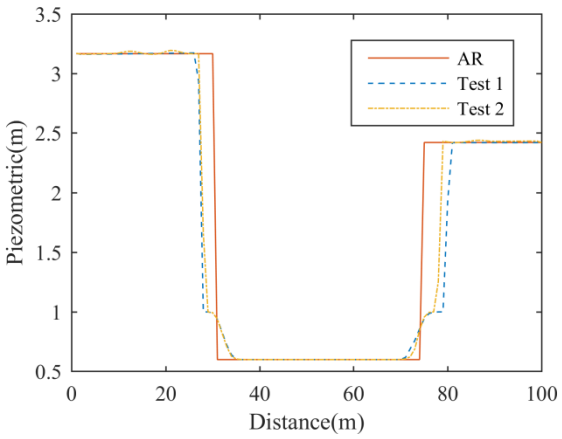

Fig 8. Simulation results of two modified HLL solvers and the analytical result (AR).

5.2. Test case 2

In test case 2, the two modified solvers are adopted to simulate a water hammer phenomenon is a 600m-long circular pipes with 0.5m diameter, the acoustic wave speed is 1200ms^{-1}. The pipe is assumed to be horizontal and frictionless, under initial condition, a flow rate of 0.477m^{3}s^{-1} is established in the pipe, a reservoir is connected at the downstream end where the water depth in it is 45m. At t = 0s, the inflow rate is decreased to 0.4m^{3}s^{-1} which produces a water hammer in the pipe, the water hammer pressure is 48.05m according to Kerger et al [26]. Two tests are conducted, the modified HLL solver proposed in this paper is adopted in test one, the values of P_a and P_b are 0.8 and 100, the modified HLL solver proposed by Malekpour et al is adopted in test 2, while the values of K_a and NS are 1.2 and 12. The simulation domain is discretized into 1000 computational cells and the time step is chosen for a Courant number of 0.8. The history of piezometric head at the upstream end of pipe in simulation results and analytical result are drawn in **Fig 9**. Two tests get almost the same results and they captured the reflection of water-hammer wave in the pipe. The L_2 of two tests are 6.3981 and 6.3986, respectively.

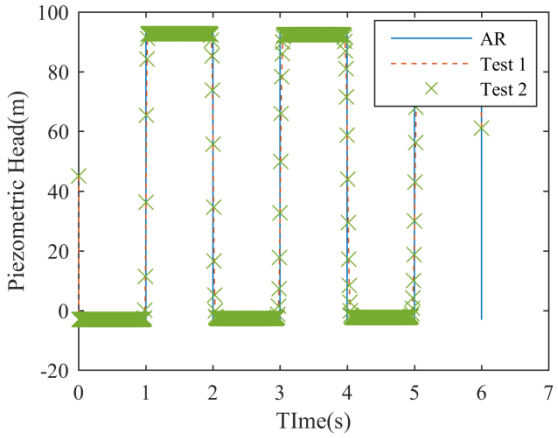

Fig 9. Simulation results of two modified HLL solvers and the analytical result (AR).

5.3. Test case 3

This experiment was carried out by Vasconcelos et al [35] to study the filling process in a realistic storm-water storage tunnel. It is a 14.6m-long horizontal tunnel with circular cross-sections of 9.4cm diameter, under initial condition, stagnant water of 7.3cm depth is established in the tunnel.

At the upstream end, a fill box with a 25cm × 25cm bottom and 31cm height above the bottom of the tunnel entrance is connected to the tunnel. At the downstream end, a surge tank with constant diameter of 19cm is connected to the tunnel. The surge is initiated by supplying constantly 3.1Ls^{-1} flow into the fill box, when the water level inside the fill box reaches its top, water is simply spilled. A gate is installed at the tunnel exit, its opening is below the water surface, when the filling bore reaches the gate and it produces large water-hammer pressure variations which damp out with time. A ventilation tower is fixed at upstream of the gate so that no air pockets occur in the tunnel. The Manning coefficient, acoustic wave speed and local head loss at the tunnel exit are 0.016m$^{1/6}$, 300ms^{-1} and 12 as suggested by Malekpour et al[24].

The modified solver proposed in this paper is adopted for numerical simulation; the values of P_a and P_b are 5 and 0.7. The simulation domain is discretized into 146 cells, the time step is set for a Courant number of 0.8. At the upstream end, the three unknowns are the discharge, the wetted area at the first cell and the water level in the fill box. At the downstream end, the three unknowns are the discharge, wetted area at the last cell and the water level at the surge tank. At the two boundaries, the continuity, energy and characteristic equations are applied to obtain the three unknowns [36]. The history of piezometric head at x = 9.9m in simulation result is depicted in Fig 10.

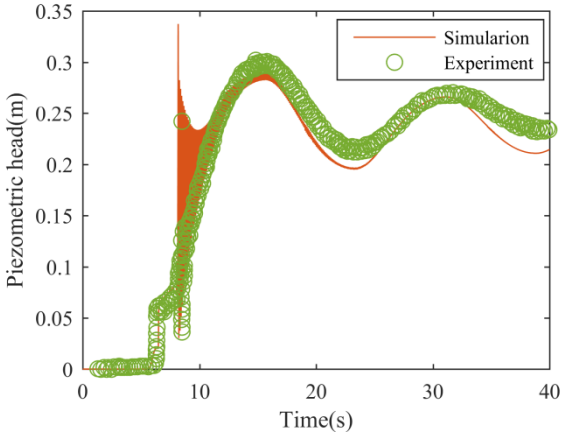

Fig 10. Simulation result of the new modified HLL solver and experimental data at x = 9.9m.

The simulation result is in good agreement with the experimental data, the new modified solver has correctly computed the arrival time of filling-bore front at x = 9.9m. The pressure oscillations triggered by the water-hammer phenomenon is nicely captured (during t = 8s ~ 10s), although the simulation result shows a longer duration time of the pressure oscillations than the experimental data. Most importantly, this case shows that the additional numerical viscosity in the new modified HLL solver does not smear the physical pressure oscillations.

5.4. Test case 4

In this test case, we study the experiment carried out by Aureli et al [25]. It is a 12.12m-long pipe with 19.2cm-diameter and 4mm-wall thickness. The pipe is divided into two parts at about 7m from the inlet, the first part has a slope of about 8.4% (downward) while the second part has a slope of -27.7%(upward). A sluice gate is installed approximately 5m from the inlet and is closed at initial condition. Six piezometric transducers are installed at the pipe bottom, their longitudinal distance to the tunnel entrance are 1m, 3m, 4.5m, 6.8m, 7.06m and 8.52m. Under initial condition, stagnant water with 22.5cm piezometric head at transducer 1 is established behind the sluice gate while other area in the pipe is dry. At the beginning of the experiment, this gate is lifted within 0.2s, sets flush into the tunnel. The tunnel entrance is blocked so that no water flows through it, while the tunnel exit is totally open.

The simulation result using the original HLL solver is referred to Aureli et al [25] where severe numerical oscillations are present. To suppress the numerical oscillations, we use the modified HLL solver proposed in this paper; the values of P_a and P_b are 4 and 0.6. The simulation domain is discretized into 303 cells, the acoustic wave speed is 200ms^{-1} and the time step is set for a Courant number of 0.8. At the upstream end, a reflective boundary condition is adopted, while a trans-missive boundary condition is adopted at the downstream end. At the boundary between wet and dry cells, the wave speed are given following Leon et al [27]. The piezometric head at x = 6.8m and x = 7.06m in simulation result are drawn in Fig 11 and Fig 12.

Preprints (www.preprints.org) | NOT PEER-REVIEWED | Posted: 24 February 2020 doi:10.20944/preprints202002.0344.v1

Peer-reviewed version available at Water 2020, 12, 1245; doi:10.3390/w12051245

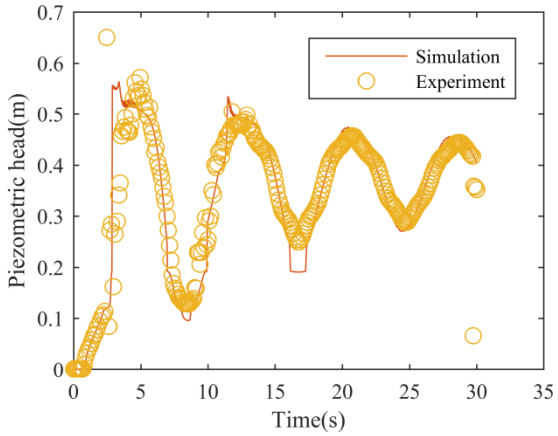

Fig 11. Piezometric head at x = 6.8m in simulation result and experimental data.

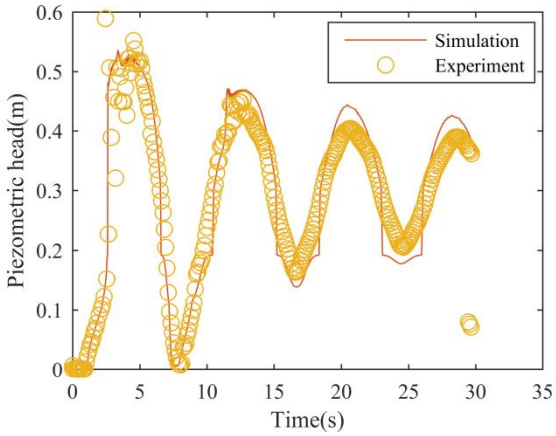

Fig 12. Piezometric head at x = 7.06m in simulation result and experimental data.

In this test case, the modified HLL solver proposed in this paper nicely captured the wetting and drying process in the pipe, the simulation result is in good agreement with the experimental data the numerical oscillations are sufficiently suppressed.

6. Conclusions

Numerical oscillations is a critical problem in transient mixed flow simulations, in this paper, some researches on the numerical oscillations are reviewed. These numerical oscillations arise from the discrepancies between the propagation of filling-bore front under realistic situations and in numerical simulations. High-order finite volume methods may cause more serious numerical oscillations, while first order finite volume methods have failed to suppress them while capturing the filling-bore front.

By now, several approaches have been proposed to suppress these numerical oscillations, their methodologies are reviewed and they are tested on a benchmark model in this paper. From their performances, we can see that the numerical oscillations can be suppressed by adding numerical viscosity. However, it is not sufficient if numerical viscosity is only admitted at the cell boundary between free-surface and pressurized regimes. Instead, to suppress the numerical oscillations, one needs to admit numerical viscosity if the water level is at the vicinity of the cross-section roof. The amount of numerical viscosity needs to be appropriate to avoid increasing the spreading length of filling-bore front. Following this idea, this paper presents a new modified HLL solver, it has two parameters, P_a needs to be larger than the highest piezometric head while P_b needs to be between 0.7 and 0.9. When the water surface is at the vicinity of cross-sectional roof, the modified solver produces larger wave speeds so that numerical viscosity is added. The amount of numerical viscosity is not sensitive to the value of P_a, one can always choose a P_a that is large enough in realistic applications.

The accuracy and robustness of this new modified solver is validated in several numerical tests. The simulation result of this new modified solver is in good agreement with the analytical result or experimental data in four test cases. The new solver has sufficiently suppressed the numerical oscillations, more importantly, it has accurately captured the propagation of filling-bore front and wet/dry interface. Compared to the modified HLL solver proposed by Malekpour et al, the solver proposed in this paper is more convenient to use and it can eliminate some minor numerical oscillations while the former one may not, see test case 1 for instance.

The result in this paper can provide useful information for readers to design an oscillation-suppressing approach. Meanwhile, one may choose the modified solver proposed in this paper or proposed by Malekpour et al alternatively to improve the accuracy and robustness in transient mixed flow simulations.

Author Contributions: Conceptualization, Zhonghao Mao, Guanghua Guan, Zhonghua Yang; Resources, Zhonghao Mao, Guanghua Guan, Zhonghua Yang; Writing – original draft, Zhonghao Mao; Writing – review & editing, Guanghua Guan.

Funding: The Authors acknowledge the support of the NSFC grant 51979202 and NSFC grant 51879199.

Acknowledgments: None.

Conflicts of Interest: None.

References

1. Cataño-Lopera, Y.A.; Tokyay, T.E.; Martin, J.E.; Schmidt, A.R.; Lanyon, R.; Fitzpatrick, K.; Scalise, C.F.; García, M.H. Modeling of a transient event in the tunnel and reservoir plan system in chicago, illinois. *Journal of Hydraulic Engineering* **2014**, *140*, 05014005.
2. Fuamba, M.; Bouaanani, N.; Marche, C. Modeling of dam break wave propagation in a partially ice-covered channel. *Advances in Water Resources* **2007**, *30*, 2499-2510.
3. Holly, F.M.; Merkley, G.P. Unique problems in modeling irrigation canals. *Journal of Irrigation and Drainage Engineering* **1993**, *119*, 656-662.
4. Guo, Q.; Song, C.C.S. Surging in urban storm drainage systems. *Journal of Hydraulic Engineering* **1990**, *116*, 1523-1537.
5. Liu, G.Q.; Guan, G.H.; Wang, C.D. Transition mode of long distance water delivery project before freezing in winter. *Journal of Hydroinformatics* **2013**, *15*, 306-320.
6. Mao, Z.H.; Guan, G.H.; Yang, Z.H.; Zhong, K. Linear model of water movements for large-scale inverted siphon in water distribution system. *Journal Of Hydroinformatics* **2019**, *21*, 1048-1063.
7. Guan, G.; Clemmens, A.J.; Kacerek, T.F.; Wahlin, B.T. Applying water-level difference control to central arizona project. *Journal Of Irrigation And Drainage Engineering* **2011**, *137*, 747-753.
8. Cong, J.; Chan, S.N.; Lee, J.H.W. Geyser formation by release of entrapped air from horizontal pipe into vertical shaft. *Journal of Hydraulic Engineering* **2017**, *143*, 04017039.
9. Liu, L.J.; Shao, W.Y.; Zhu, D.Z. Experimental study on stormwater geyser in vertical shaft above junction chamber. *Journal of Hydraulic Engineering* **2020**, *146*.
10. Chegini, T.; Leon, A.S. Numerical investigation of field-scale geysers in a vertical shaft. *Journal of Hydraulic Research*.
11. Cunge, J.A.; Wegner, M. Intégration numérique des équations d'écoulement de barré de saint-venant par un schéma implicite de différences finies. *Houille Blanche-revue Internationale De L Eau* **1964**, 33-39.
12. An, H.; Lee, S.; Noh, S.J.; Kim, Y.; Noh, J. Hybrid numerical scheme of preissmann slot model for transient mixed flows. *Water* **2018**, *10*, 899.
13. Dazzi, S.; Maranzoni, A.; Mignosa, P. Local time stepping applied to mixed flow modelling. *Journal of Hydraulic Research* **2016**, *54*, 145-157.
14. Fernandez-Pato, J.; Garcia-Navarro, P. A pipe network simulation model with dynamic transition between free surface and pressurized flow. In *12th international conference on computing and control for the water industry, ccwi2013*, Brunone, B.; Giustolisi, O.; Ferrante, M.; Laucelli, D.; Meniconi, S.; Berardi, L.; Campisano, A., Eds. Elsevier Science Bv: Amsterdam, 2014; Vol. 70, pp 641-650.
15. Kerger, F.; Erpicum, S.; Dewals, B.J.; Archambeau, P.; Pirotton, M. 1d unified mathematical model for environmental flow applied to steady aerated mixed flows. *Adv. Eng. Softw.* **2011**, *42*, 660-670.
16. Ferreri, G.B.; Freni, G.; Tomaselli, P. Ability of preissmann slot scheme to simulate smooth pressurisation transient in sewers. *Water Science and Technology* **2010**, *62*, 1848-1858.
17. Maranzoni, A.; Mignosa, P. Numerical treatment of a discontinuous top surface in 2d shallow water

mixed flow modeling. *International Journal for Numerical Methods in Fluids* **2018**, *86*, 290-311.

18. Maranzoni, A.; Dazzi, S.; Aureli, F.; Mignosa, P. Extension and application of the preissmann slot model to 2d transient mixed flows. *Advances in Water Resources* **2015**, *82*, 70-82.
19. Toro, E.F.; Garcia-Navarro, P. Godunov-type methods for free-surface shallow flows: A review. *Journal of Hydraulic Research* **2007**, *45*, 736-751.
20. Kitamura, K.; Shima, E. Numerical experiments on anomalies from stationary, slowly moving, and fast-moving shocks. *Aiaa J.* **2019**, *57*, 1763-1772.
21. Johnsen, E. Analysis of numerical errors generated by slowly moving shock waves. *Aiaa J.* **2013**, *51*, 1269-1274.
22. R, D.W.Z.a.P.L. Flux functions for reducing numerical shockwave anomalies. In *Seventh International Conference on*

Computational Fluid Dynamics, Big Island, Hawaii, 2012.

23. Vasconcelos, J.G.; Wright, S.J.; Roe, P.L. Numerical oscillations in pipe-filling bore predictions by shock-capturing models. *Journal of Hydraulic Engineering* **2009**, *135*, 296-305.
24. Malekpour, A.; Karney, B.W. Spurious numerical oscillations in the preissmann slot method: Origin and suppression. *Journal of Hydraulic Engineering* **2016**, *142*, 04015060.
25. Aureli, F.; Dazzi, S.; Maranzoni, A.; Mignosa, P. Validation of single- and two-equation models for transient mixed flows: A laboratory test case. *Journal of Hydraulic Research* **2015**, *53*, 440-451.
26. Kerger, F.; Archambeau, P.; Erpicum, S.; Dewals, B.J.; Pirotton, M. An exact riemann solver and a godunov scheme for simulating highly transient mixed flows. *Journal of Computational and Applied Mathematics* **2011**, *235*, 2030-2040.
27. Leon, A.S.; Ghidaoui, M.S.; Schmidt, A.R.; Garcia, M.H. Application of godunov-type schemes to transient mixed flows. *Journal of Hydraulic Research* **2009**, *47*, 147-156.
28. Vasconcelos, J.G.; Wright, S.J.; Roe, P.L. Improved simulation of flow regime transition in sewers: Two-component pressure approach. *Journal of Hydraulic Engineering* **2006**, *132*, 553-562.
29. Kim, S.S.; Kim, C.; Rho, O.H.; Hong, S.K. Cures for the shock instability: Development of a shock-stable roe scheme. *Journal of Computational Physics* **2003**, *185*, 342-374.
30. Toro, E. *Shock capturing methods for free surface shallow water flows*. 2002.
31. Leon, A.S.; Ghidaoui, M.S.; Schmidt, A.R.; Garcia, M.H. Godunov-type solutions for transient flows in sewers. *Journal of Hydraulic Engineering-Asce* **2006**, *132*, 800-813.
32. Toro, E.F.; Billett, S.J. Centred tvd schemes for hyperbolic conservation laws. *Ima Journal of Numerical Analysis* **2000**, *20*, 47-79.
33. Toro, E.F.; Hidalgo, A.; Dumbser, M. Force schemes on unstructured meshes i: Conservative hyperbolic systems. *Journal of Computational Physics* **2009**, *228*, 3368-3389.
34. Bertaglia, G.; Ioriatti, M.; Valiani, A.; Dumbser, M.; Caleffi, V. Numerical methods for hydraulic transients in visco-elastic pipes. *Journal of Fluids and Structures* **2018**, *81*, 230-254.
35. Vasconcelos, J.; Wright, S. *Experimental investigation of surges in a stormwater storage tunnel*. 2005; Vol. 131.
36. Vasconcelos, J.; Wright, S. *Numerical modeling of the transition between free surface and pressurized flow in storm sewers*. 2004.